Impact of Horizontal Resolution

on summer monsoon Precipitation

Simulation over the Korean Peninsula

using Two-way Nesting Method

by

Gaeun Kim

Department of Environmental and Atmospheric Sciences

The Graduate School

Pukyong National University

February 23, 2018

Impact of Horizontal Resolution
on summer monsoon Precipitation Simulation
over the Korean Peninsula
using Two-way Nesting Method

(양방향 둥지격자기법을 활용한 한반도 여름철

강수모의에서 수평해상도의 영향)

Advisor: Prof. Jai-Ho Oh

by

Gaeun Kim

A thesis submitted in partial fulfillment of the requirements
for the degree of

Master of Science

in Department of Environmental and Atmospheric Sciences,

The Graduate School, Pukyong National University

February 2018

Impact of Horizontal Resolution
on summer monsoon Precipitation Simulation
over the Korean Peninsula
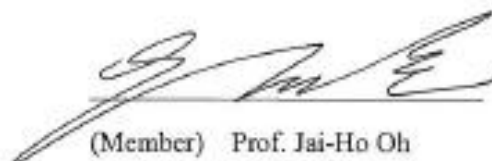# using Two-way Nesting Method

A dissertation

by

Gaeun Kim

Approved by:

_____

(Chairman) Prof. Won-Sik Choi

_____
(Member)   Dr. R.H. Kriplani

_____
(Member)   Prof. Jai-Ho Oh

February 23, 2018

Contents

List of Figures

List of Tables

양방향 둥지격자기법을 활용한 한반도 여름철 강수모의에서

수평해상도의 영향

김가은

부경대학교 대학원 환경대기과학과

요약

특정한 지역의 상세 기후정보를 생산하기 위해 사용하는 가장 보편적인 기술은 지역 기후모델을 이용하는 것이며 많은 연구자들이 지역기후 모델을 이용하여 한반도의 강수모의에 수평해상도가 미치는 영향에 대해 연구한 바 있다 (Lee at al. 2008, Sung et al. 2014, Kim et al. 2016). 그러나 이러한 방법은 추가적인 내삽과정을 필요로 하고 (Wu et al. 2004), 서로 다른 두 모델이 서로 다른 특성을 가지기 때문에 에러를 유발할 수 있음이 밝혀진 바 있다 (Leung et al. 2003). 위와 같은 에러는 고해상도 전지구 모델을 이용하거나, grid nesting 기법을 이용하는 등의 방법으로 피할 수 있으나, 고해상도의 전지구 모델을 이용하는 경우에는 전산자원 활용의 관점에서 다소 비현실적일 수 있다는 한계점이 있다.

본 연구에서 사용된 모델은 독일의 현업모델인 ICON 모델로서 비정역학 코어를 사용하며, 전 지구를 정20면체 격자로 표현한다. 또한 two-way nesting 기법을 적용할 수 있어 앞서 언급한 문제점을 피할 수 있는 장점이 있다. 따라서, 본 연구에서는 ICON 모델에서 two-way nesting 기법을 활용하여 한반도 여름 몬순 강수를 전지구 40-km, 동아시아 10-km로 모의하고 수평해상도의 영향을 알아보았다. RMSE와 Pearson Correlation Coefficient, Student's t-test, Contingency table 등이 모델 결과자료를 비교하기 위해 이용되었고, 그 결과에서 상세 도메인에서 지형효과에 의한 강수분포가 더 잘 나타남을 확인 할 수 있었다. 또한 two-way nesting을 적용하지 않은 실험과 비교했을 때, 모델 기후값에는 큰 차이가 없었으나 상세 도메인에서 전지구 도메인으로의 피드백 효과에 따라 two-way nesting을 적용한 실험에서 관측과의 오차가 줄어들며, 강수유무를 보다 잘 모의하는 것으로 나타났다.

I. Introduction

The most common technique to produce a detailed climate for selected regions is using Regional Climate Models (RCMs). A regional model is initialized by global model output and forced at its lateral boundaries.

Many researches have been conducted with this method to define the impact of horizontal resolution on precipitation over the Korean peninsula. Lee et al. (2008) noted the regional climate model with higher resolution simulates more precipitation over the Korean peninsula compared to the lower resolution one reducing the systematic bias. Seong et al. (2014) compared two regional climate simulation by changing its boundary data and evaluated their simulation skills of fine-scale climate. Kim et al. (2016) revealed that increase of horizontal resolution could improve the duration and the amount of precipitation using multiple RCMs.

However, there is the necessity of additional interpolation to preprocess the global data onto the regional grid (Wu et al., 2004). Leung et al. (2003) mentioned the limitation that the two different model might have different numerical method and parameterizations, or even different dynamical core so that this inconsistency could cause an error when propagating into the regional domain. Kim (2010) showed the result of the regional climate model could be different following the location and the size of a domain even though it forced by the same global data.

Problems with lateral boundary conditions can be averted by using a high-resolution global grid, grid nesting (Harris and Durran, 2010), and so forth. Kitoh and Kusunoki (2008) revealed 20-km mesh AGCM shows the better orographic rainfall not only the location but also the amount of precipitation during East Asia Summer Monsoon by comparing it to 180-km mesh AGCM. However, simulating the whole globe with 20-km resolution can be impractical given current computational limitation. Harris and Lin (2014) demonstrated the precipitation on the nested grid could improve the representation of fine-scale features and reduce existing model biases over the Maritime continent and North America.

Therefore, in this study, summer monsoon prediction over the Korean peninsula with the horizontal resolution of 40-km (global) and 10-km (nested domain) using two-way nesting method will be simulated, and the impact of horizontal resolution will be shown by comparing them to one another.

II. Model and Experiment

1. Model description

The atmospheric general circulation model used in this study is an icosahedral non-hydrostatic (ICON) model. The ICON model is developed under a collaboration between the Deutscher Wetterdienst (DWD) and Max-Plank Institute for Meteorology (MPI-M) to build a unified modeling system for numerical weather prediction and climate modeling. This project also aimed to get better conservation properties than in existing global models, applicability on a various range of scales from ~100-km to ~1-km, and the possibility of static mesh refinement and nesting.

The ICON model employs non-hydrostatic dynamical core on a spherical icosahedral grid obtained by projecting and subdividing an icosahedron, which consists of 20 equilateral triangles of equal sizes. Icosahedron allows to avoid so-called pole problem exists in conventional latitude-longitude grids by representing two of the twelve vertices to the North and South poles. The rest five vertices on each hemisphere locate along the latitude circle of 26.6˚ and 26.6˚S having longitude intervals of 72˚.

By refining each face of the spherical icosahedral grid, the grid can be distinguishable as either equilateral triangles or hexagonal/pentagonal cells of equal size. In the root division step, the great circle arcs forming the edges of the core

triangles (parent cells) are divided into n equal arcs per edge (Rn). Connecting the new edge points with great circle arcs yields n^2 triangles within the original triangle. This step may repeat for k bisection steps (Bk), where each triangle is subdivided into four smaller triangles (Fig. 1). This process is called as $RnBk$ grid, and some commonly used grids are in Table 1.
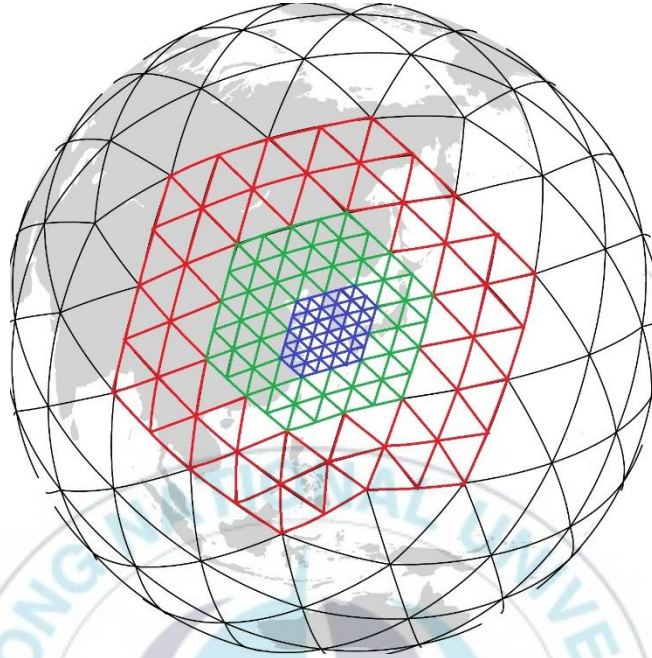
Figure 1 Illustration of the grid construction procedure. Black line denotes R02B01, red line denotes R02B02, green line denotes R02B03, and blue line denotes R02B04.

Table 1. The number of cells and edges, effective grid resolution and maximum/minimum cell area ration of the grids.

Grid	Number of cells	Number of edges	Effective grid resolution (km)	Max/Min cell area ratio
R2B04	20,480	30,720	157.8	1.38
R2B05	81,920	122,880	78.9	1.44
R2B06	327,680	491,520	39.5	1.49
R2B07	1,310,720	1,966,080	19.7	1.53

While a triangular cell can be divided into sub-triangles, a hexagonal cell cannot be correctly overlapped a set of hexagons at a higher resolution. This hierarchical structure of the triangular mesh is favorable for the implementation of mass conserving discretization for multi-resolution capabilities such as one-way and two-way nesting.

The grid-nesting approach applied to ICON model is a two-way nesting. The mesh-size ratio is fixed to a value of 2 which implies that one large triangular cell (parent cell) is subdivided into four small triangular cells (child cells) to avoid the problem of unphysical wave reflections at the nest boundaries. The time step in the nested domain(s) is reduced according to the mesh refinement ratio to assure numerical stability with time stepping. The nesting tasks for multiple levels and multiple nested domains are allowed. Additionally, vertical nesting is also available allowing that a nested domain may have a lower top level than the parent domain. At each model runtime, the model integrates one physics time step in the parent domain and two physics time step in the nested domain(s). It also provides the feedback from the nested domain(s) to the parent domain by applying bilinear interpolation. A more detailed description of the ICON model is provided by Zangl et al. (2015).

2. Experimental Design

Two Atmospheric Model Intercomparison Project (AMIP) type experiments have been performed to produce the model climatology. One is without two-way nesting, and the other is with two-way nesting. The horizontal resolution of the global grid in both experiments is same as 40-km, and the vertical resolution is 90 levels up to 75-km height. Both experiments are run for 31 years during 1979-2009.

The ICON model, one of the Atmospheric Global Circulation Models (AGCMs), takes prescribed monthly sea surface temperature (SST) and sea ice concentration (SIC) as the lower boundary conditions (Hurrell et al., 2008) since the AGCMs cannot predict the ocean condition.

The two-way nesting simulation took the global domain as the mother domain and adopted two nested (child) domains. The second domain (the first child domain) covers Asia from India, the leftmost, to Western Pacific (60-180˚E, 10˚S-60˚N) with the horizontal resolution of 20-km (R2B7). The third domain (the second child domain) covers East Asia centered on the Korean peninsula (100-150˚E, 20˚N-50˚N) with the horizontal resolution of 10-km (R2B8), and it comes under the second domain. The vertical resolution of all domains is 90 levels up to 75-km height.

Figure 2 shows the layout of the domains and Table 2 gives a glance of domain composition. Table 3 gives a glossary of the terms naming each experiment to clarify.
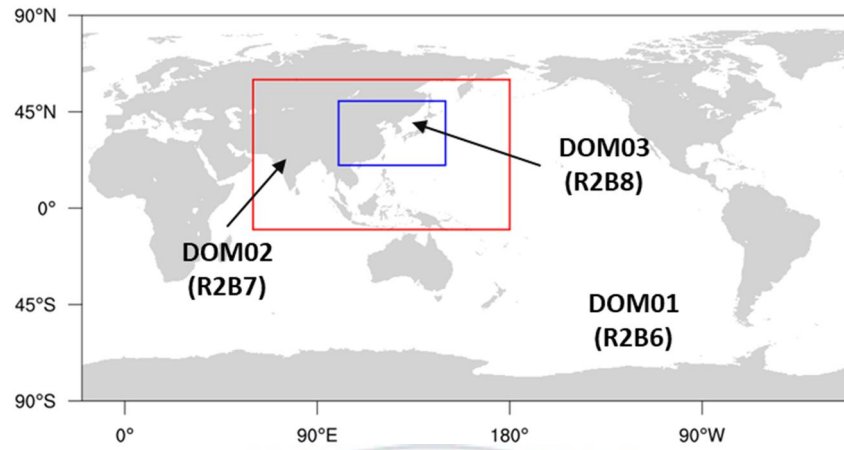
Figure 2 Layout of domain composition. The area inside of the red line is the second domain (the first child domain), and the area inside of the blue line is the third domain (the second child domain).

Table 2. Range and resolution of each domain.

	Without nesting	With two-way nesting		
Domain	Global	Global (DOM01)	Asia (DOM02)	Korea (DOM03)
Lat/Lon range	-	-	60-180˚E, 10˚S-60˚N	100-150˚E, 20˚N-50˚N
Horizontal resolution	40-km	40-km	20-km	10-km
Vertical resolution	90 levels up to 75-km			
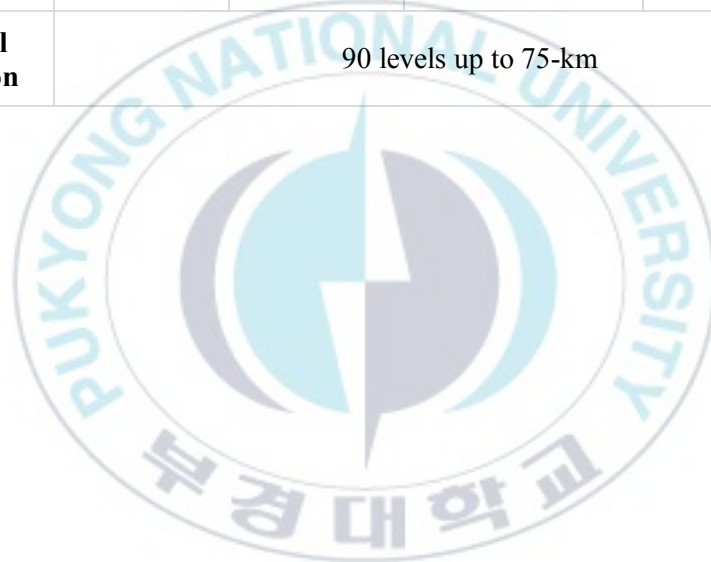
Table 3 A glossary of the terms naming each experiment

Domain	Global	Global (DOM01)	Korea (DOM03)
Nesting applied or not	Not applied	Applied	
Experiment name	ICON w/o nesting	ICON 2way 40-km	ICON 2way 10-km

3. Observational Data

For the model verification, several precipitation datasets are used. Those are the ERA-Interim (Dee et al. 2011), the Tropical Rainfall Measuring Mission (TRMM) 3B43 (Huffman et al. 2007), the Asian Precipitation Highly-Resolved Observational Data Integration Towards Evaluation (APHRODITE), and the synthetic observational precipitation data (1-km resolution) (Bae et al. 2017). The ERA-Interim (T255, about 80-km resolution) dataset is also used for comparing atmospheric circulation fields.
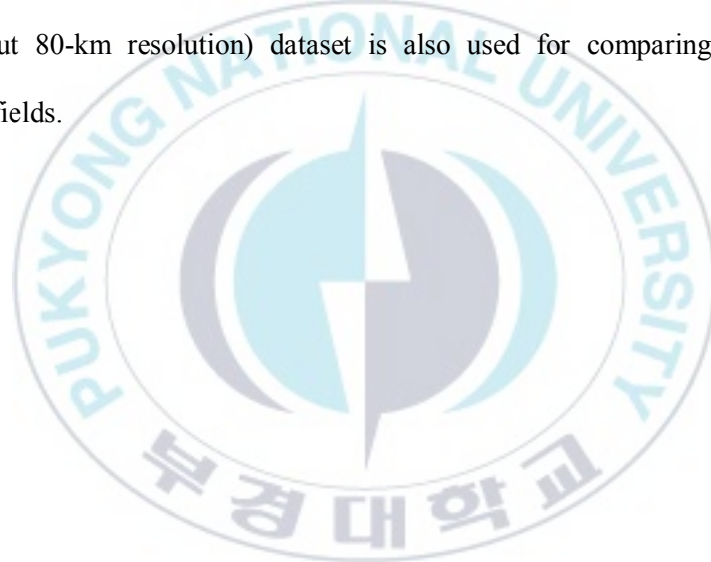
4. Analysis method

Boreal summer seasonal (June-July-August, JJA) mean precipitation of the ICON model is compared to the other datasets regarding spatial distribution, and zonal distribution after approving that the two climatology is not remarkably different. The latitude-height cross section for vertical wind is compared to ERA-Interim dataset.

The RMSE measures the difference between predicted values from a model or an estimation and actual observed values. Thus, RMSE is a measure of accuracy comparing forecasting errors of different models.

$$RMSE = \sqrt{\frac{1}{M} \sum_{m=1}^{M} [(x_m - \bar{x}) - (y_m - \bar{y})]^2} \qquad (2.4.1)$$

$$NRMSE = \frac{RMSE}{y_{max} - y_{min}} \qquad (2.4.2)$$

Where M is the number of grids, $\bar{x}$ and $\bar{y}$ are the climatological value of the forecast(x_m) and observation(y_m) at each grid point. RMSE always has a positive value, and zero means perfect forecast.

The Pearson Correlation Coefficient, as known as the Pearson's r, is used to measure the linear correlation between the two simulations in 40-km resolution. It

ranges from -1 to 1, where -1 is a total negative linear correlation, 0 is no linear correlation, and 1 is a total positive correlation. The formula for r is as below:

$$r = \frac{\sum_{i=1}^{n}(x_i - \bar{x})(y_i - \bar{y})}{\sqrt{\sum_{i=1}^{n}(x_i - \bar{x})^2}\sqrt{\sum_{i=1}^{n}(y_i - \bar{y})^2}} \qquad (2.4.3)$$

The student's T-test is utilized to compare two averages of the two 40-km resolution experiments. The student's T-test tells whether the two averages are different from each other, and how significant the differences are.

The Contingency Table analysis is used to verify and compare the existence and the nonexistence of precipitation in each experiment. The Contingency Table is mostly used to evaluate dichotomous variables. In this table, hits (H) state both observation and simulation detect the event, whereas misses (M) indicate the events only identified by the observation. False (F), also known as the false alarm, means the event is determined by the simulation but not confirmed by the observation. Finally, Correct Negatives (R) indicate both the observation and the simulation have no event existence.

Table 4 The contingency table.

		Simulation	
		Yes	No
Observation	Yes	H (hits)	M (misses)
	no	F (false)	R (correct negatives)

Usually, the Accuracy (ACC) of the dichotomous variables describes the ratio of right guess regardless of the existence of the event among the total sample. The range of ACC is between 0 and 1. The closer to 1, the more accurate.

$$ACC = \frac{H + R}{H + M + F + R} \quad (2.4.3)$$

The Probability of Detection (POD) expresses a fraction of the observation detected correctly by the simulation. POD ranges from 0 to 1, and the perfect score has the value of 1.

$$POD = \frac{H}{H + M} \quad (2.4.4)$$

The False Alarm Ratio (FAR) speaks for a fraction of events identified by simulation but not confirmed by the observation. FAR has the value between 0 and 1, 0 means the perfect score.

$$FAR = \frac{F}{H + F} \quad (2.4.5)$$

The Critical Success Index (CSI) combines the different aspect of the POD and FAR, representing the overall skill of the simulation relative to the observation. The CSI ranges from 0 to 1, 1 indicates perfect skill.

$$CSI = \frac{H}{H + M + F} \quad (2.4.6)$$

III. Results

1. Model climatology comparison

The model climatology both with and without two-way nesting have been compared. Figure 3, figure 4 and figure 5 show the latitude-height cross section of JJA mean (1979-2009) zonally averaged temperature, zonal wind, and vertical wind in ICON w/o nesting and ICON 2way 40-km with the difference between them.

After applying two-way nesting, the temperature over the polar region has been slightly decreased (about 0.6℃) (Fig. 3). The zonal wind in the southern hemisphere has changed. Slight increase signal (about 1.5 m/s) over the equator and the south pole, and decrease signal (about 1.5 m/s) over 60°N has appeared (Fig. 4). The vertical wind has not much changed. The maximum difference of the vertical wind was 0.001 pa/s, and the minimum was -0.001 pa/s (Fig. 5).

Despite there were minor changes, the two-way nesting simulation did not appreciably distort the zonal mean temperature and wind compared to the without two-way nesting simulation.
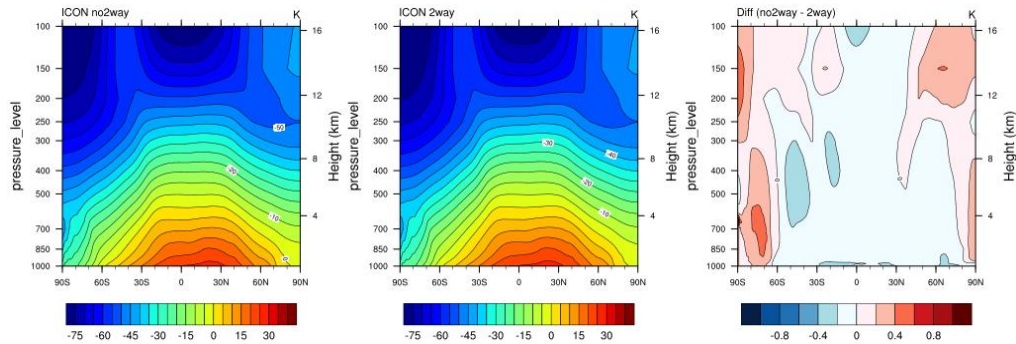
Figure 3 Latitude-Height cross section of JJA mean (1979-2009) zonally averaged temperature. (left) ICON w/o 2way, (middle) ICON 2way, and (right) difference (ICON w/o 2way – ICON 2way).
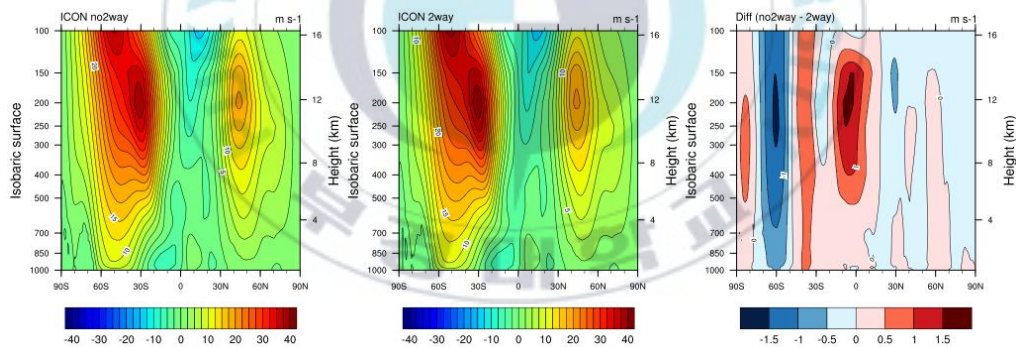
Figure 4 Same as figure 3, but zonally averaged zonal wind.

1 8
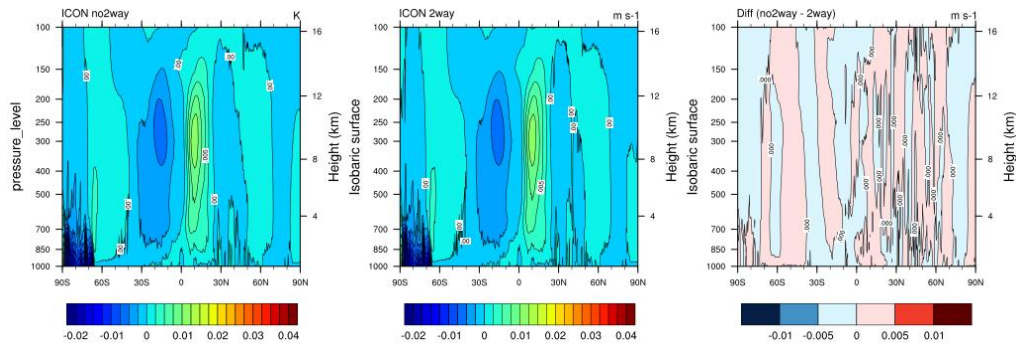
Figure 5 Same as figure 3, but zonally averaged vertical wind.

2. Effect of horizontal resolution increase

Figure 6 shows the topography used in 40-km resolution and 10-km resolution experiment. The highest peak in the presented domain is 1550-m in 40-km resolution and 1771-m 10-km resolution. A couple of peaks in North Korea which is not evident in 40-km resolution is revealed in 10-km resolution. Moreover, Sobaek mountains and the Taebaek mountains appear more clearly in 10-km resolution. Likewise, the mountain Hala is recognizable in 10-km resolution.

a) Geometric height in 40km resolution m

b) Geometric height in 10km resolution m

100 250 400 550 700 850 1000 1150 1300 1450 1600 1750 1900
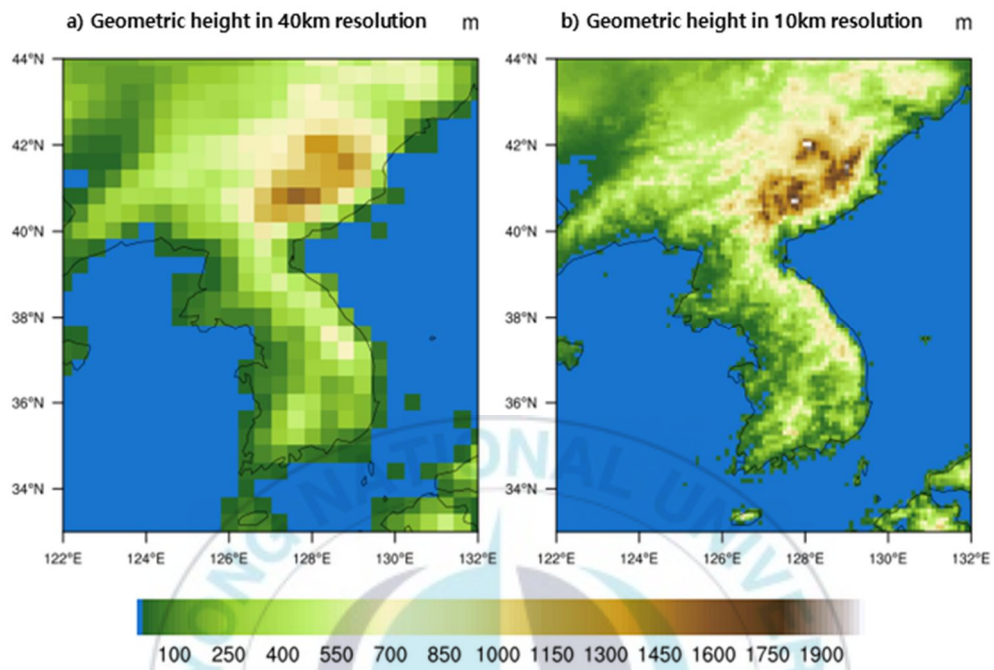
Figure 6 Geometric height (meter) in a) ICON 40-km resolution,

and b) ICON 10-km resolution

Simulated June-July-August (JJA) mean precipitation of 8 years' climatology (2000-2007) from the two versions of simulations, without two-way nesting and with two-way nesting, are compared with other datasets.

Figure 7 shows the spatial distribution of JJA mean precipitation (mm/day) over Asia, and the latitude and longitude range is same as 20-km resolution domain (60-180˚E, 10˚S-60˚N). Both the nesting applied and not applied versions captured significant convection over the eastern Arabian Sea, the Bay of Bengal, the South China Sea, and the Philippines Sea, and southwestern part of Japan. However, ICON model has overestimated regarding the magnitude of precipitation. Relatively low rainfall over the southeastern part of the Indian peninsula is also well simulated. Compared to the nesting not applied version, the nesting applied version simulated more successfully the narrow precipitation bands windward of the mountain Himalayas. There are high rainfalls over the western side of mountains of the Western Ghats, the Gulf of Thailand together with lee-wind side precipitation minima over Indochina peninsula, and the Philippines.

Figure 8 shows the spatial distribution of JJA mean precipitation (mm/day) over the Korean peninsula. Further, synthetic observational precipitation data and ICON two-way 10-km are shown along with others. As the horizontal resolution increases, the narrow precipitation band along the Taebaek mountains and precipitation over the north-west part of North Korea are noticeable in ICON 2way 10-km, which are not evident in other datasets except the synthetic observational precipitation data. The

2 2

precipitation over Jeju island, the most precipitation is produced by the mountain Hala is also noticeable in 10-km resolution.
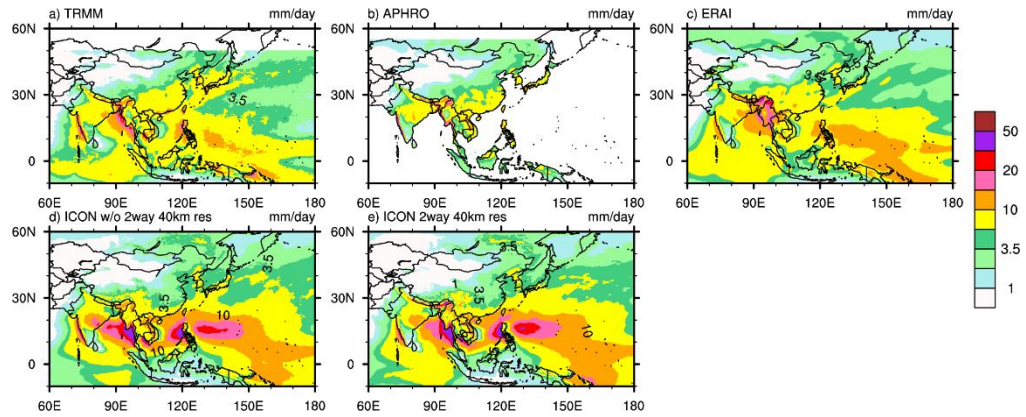
Figure 7 JJA mean precipitation (2000-2007) over Asia in mm/day. The latitude and longitude range is same as 20-km resolution domain (60-180˚E, 10˚S-60˚N). a) TRMM, b) APHRODITE, c) ERA-interim, d) ICON w/o nesting and e) ICON 2way 40-km.

Figure 8 JJA mean precipitation (2000-2007) over Korean peninsula (122-132˚E, 33˚S-44˚N) in mm/day. a) TRMM, b) APHRODITE, c) ERA-interim, d) Synthetic precipitation data, e) ICON w/o nesting, f) ICON 2way 40-km, and g) ICON 2way 10-km.

The zonal distribution of JJA mean precipitation for ten years (1998-2007) along 35.3˚N is displayed in Figure 9 to see topography-related precipitation. The yellow line denotes the ICON 2way 10-km, the cyan line denotes the ICON 2way 40-km, and the red line denotes the ICON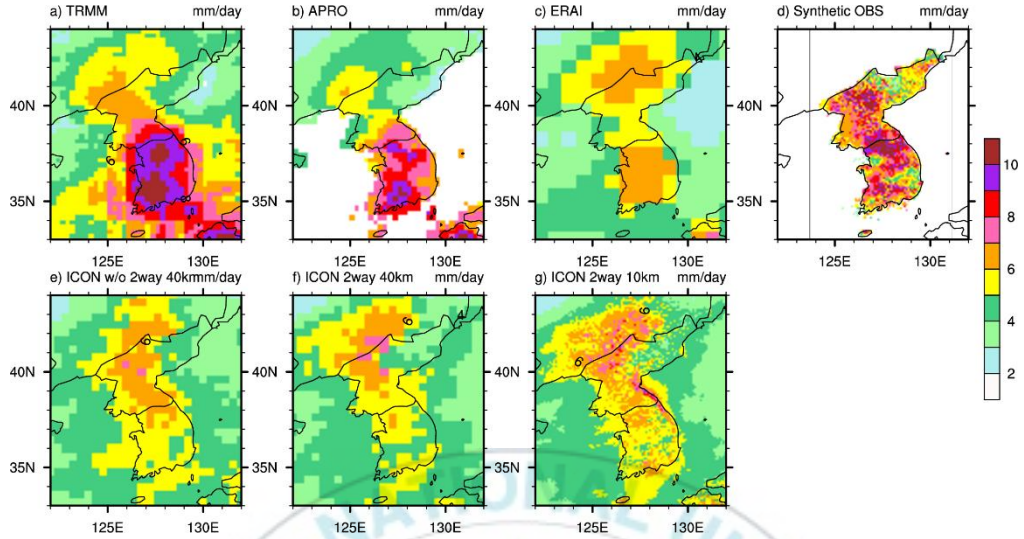 w/o 2way. The observations and reanalysis are shown in different colors (green for ERA-Interim, pink for TRMM, and blue for APHRODITE, respectively). Topography cross-section in each resolution of ICON model is also plotted.

All observations show a distinct peak of ~11 mm/day at Mt. Jiri (127˚E). The ICON 2way 10-km reproduces this peak well, compared to the ICON w/o 2way (~5 mm/day). Moreover, there is an improvement in the ICON 2way 40-km (~6 mm/day) by getting feedback from its nested domain.

In topography cross-section plot, the highest point of Mountain Sobaek in 10-km resolution differ more than twice from that of 40-km resolution. This difference may affect precipitation simulation corresponding to the local orography.
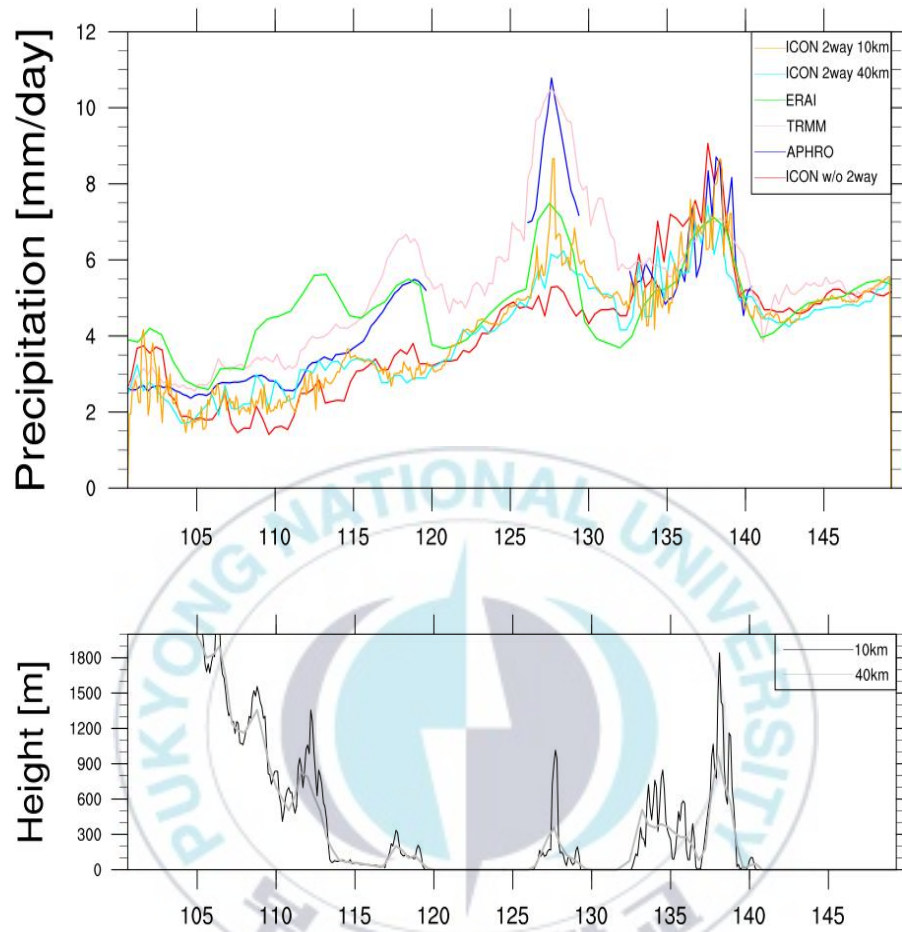
Figure 9 JJA mean precipitation (1998-2009) in mm/day along 35.3˚N. Topography cross section is also shown.

The Changma rain band is the most distinct characteristic of Korea summer climate, making July the wettest month. The Changma front structure is shown in Figure 10 regarding the latitude-height cross sections of vertical winds in July at 127˚E based on ERA-Interim. The Same figure but based on ICON w/o 2way is in Figure 11, ICON 2way 40-km is in Figure 12, and ICON 2way 10-km is shown in Figure 13.

The ERA-Interim shows an intense upward motion (> -0.02 Pa s^{-1} from 30˚N to northwards, 850 hPa) exists in the lower-troposphere and extends up to about 100 hPa. The ICON model basically reproduced this characteristics, moreover, downward motion derived from local orography appears.

The weak upward motion at 30˚N in ICON w/o 2way disappears in ICON 2way 40-km. The downward motion at 40˚N, 850 hPa became stronger in ICON 2way 40-km, compared to ICON w/o 2way. The ICON 2way 10-km shows stronger orographical downward motion, compared to the ICON 2way 40-km. This difference seems to arise from the detailed topography in 10-km resolution and the feedback from the child domain (10-km) to mother domain (40-km).
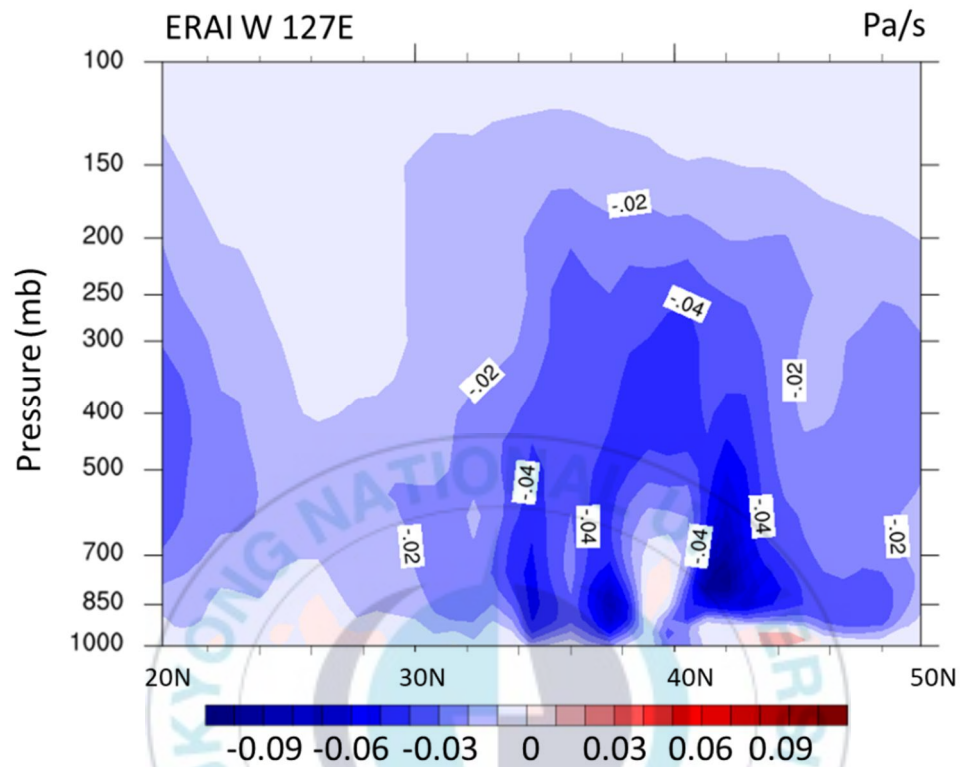
Figure 10 latitude-height cross sections of vertical winds in July at 127˚E based on ERA-Interim.
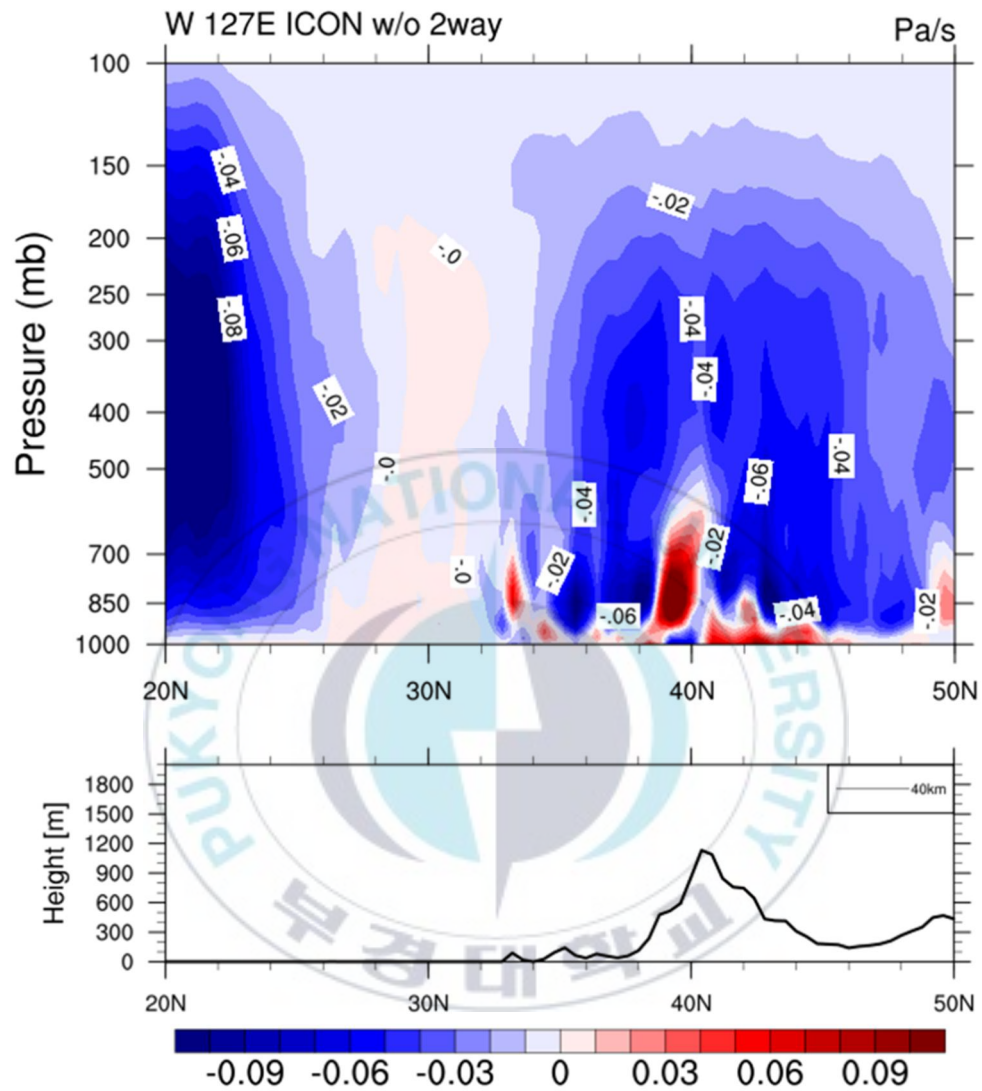
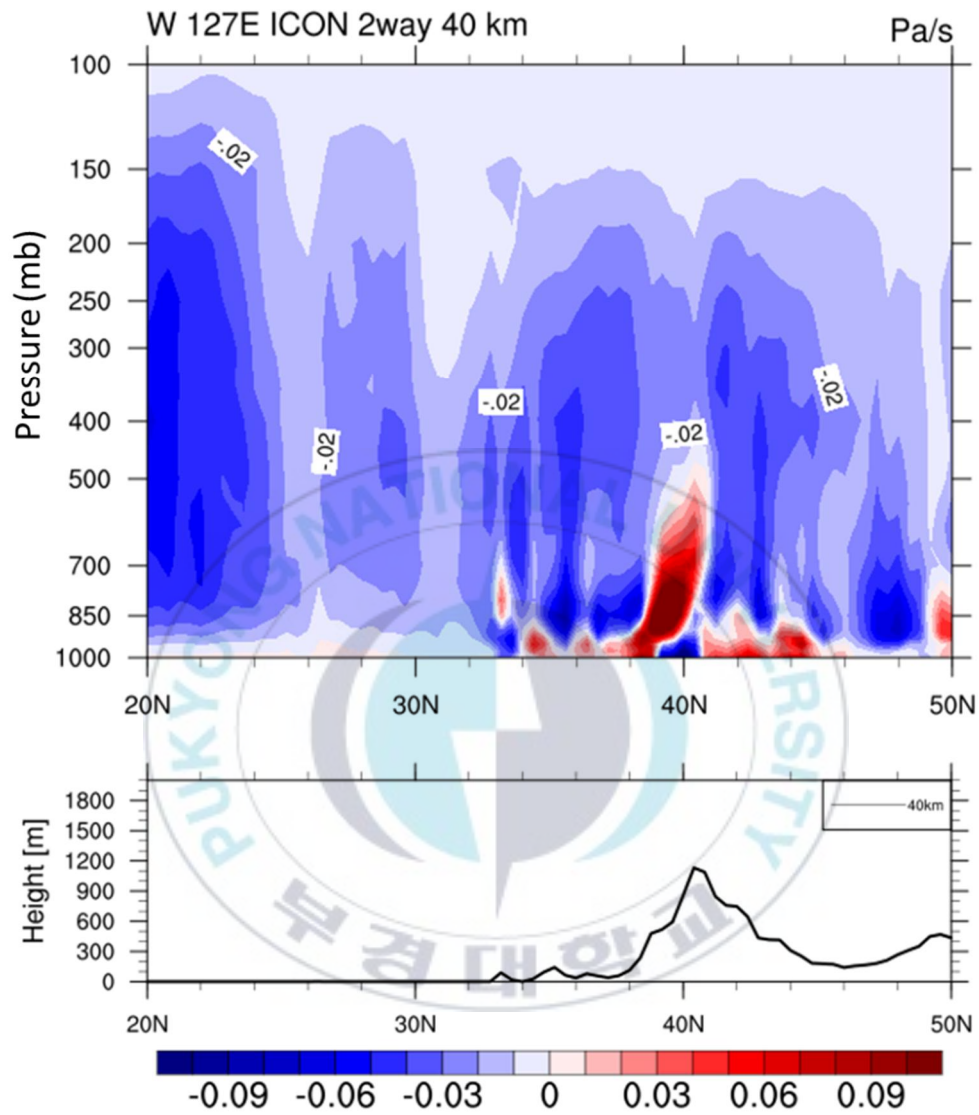**Figure 11 Same as figure 7 but based on ICON w/o 2way version.**

Figure 12 Same as figure 7 but based on ICON 2way 40-km version.
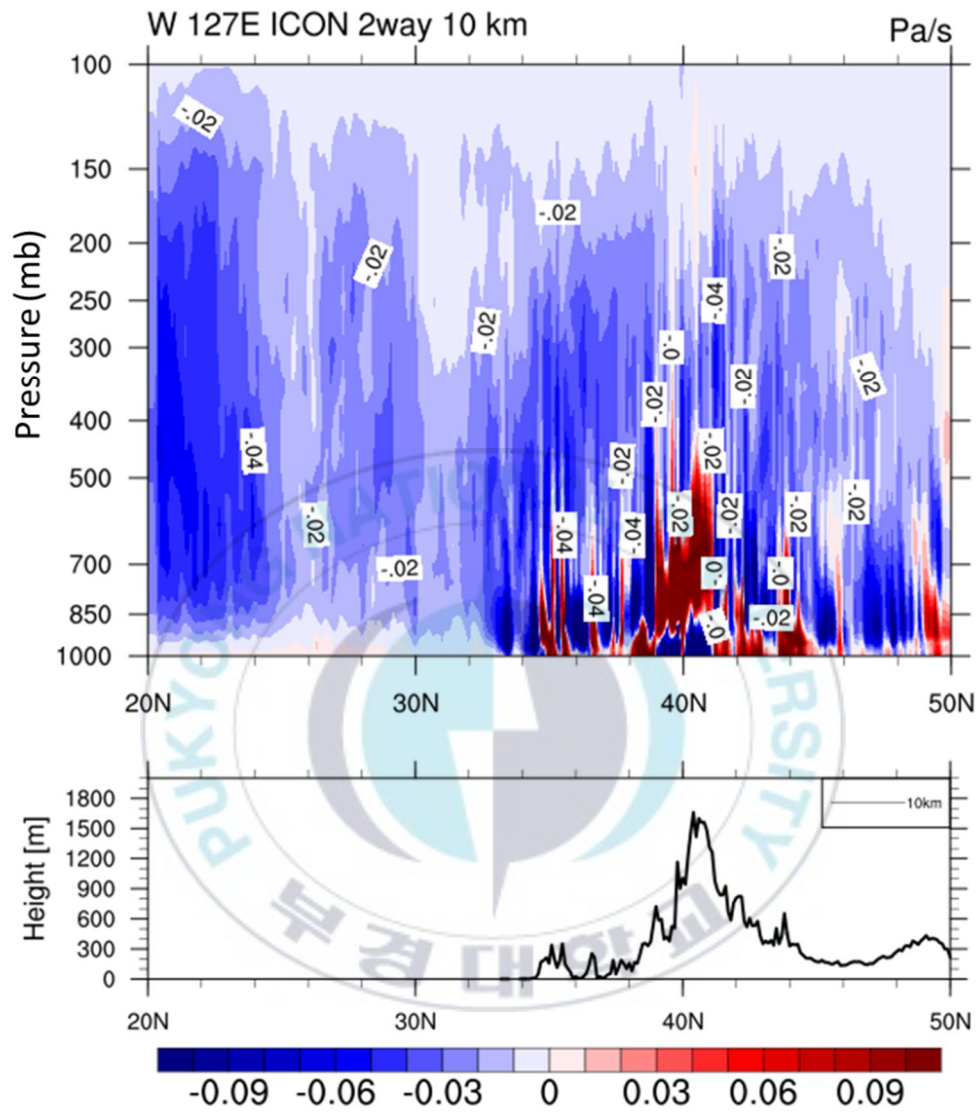
Figure 13 Same as figure 7 but based on ICON 2way 10-km version.

The NRMSE (%) with Student's t-test and Pearson correlation coefficient with Student's t-test are applied to assess the difference between the climatological precipitation (31years, 1979-2009) of the two 40-km simulations and ERA-Interim (Figure 14). The ERA-Interim is linearly interpolated to 40-km resolution for the calculation.

The NRMSE dropped over South Korea, Japan, and southeastern part of China after applying the two-way nesting method (Figure 14 (a) and (b)). Additionally, the p-value rises at the Eastern sea, so it became significant at confidence level of 95%

The Pearson Correlation Coefficient also mostly rises after applying the two-way nesting method. It rises to 0.7 over the Korean peninsula, along with the slight improvement over the East Sea and the East China Sea. Likewise, the Western Pacific is also improved and became significant at the confidence level of 95% (Figure 14 (c) and (d)).

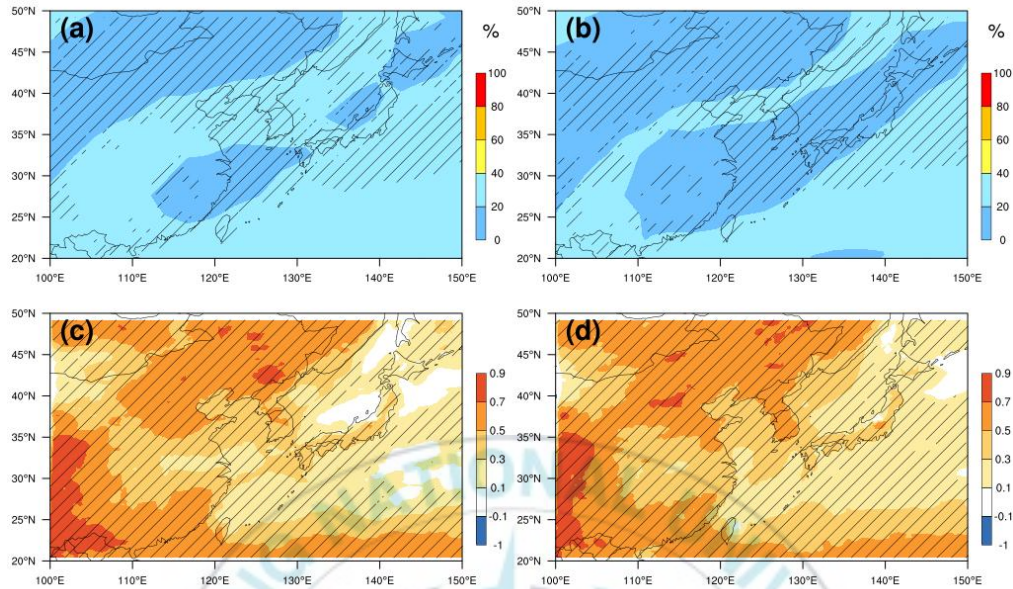**Figure 14 NRMSE (%) and Student's t-test for climatological precipitation (31years, 1979-2009) between ERA-Interim and (a) ICON w/o 2way, (b) ICON 2way 40-km. Pearson correlation coefficient with Student's t-test between ERA-Interim and (c) ICON w/o 2way, (d) ICON 2way 40-km. Shaded denotes NRMSE (%), and a deviant crease line denotes a significant level of 95% (p-value > 0.05) using Student's t-test**

The contingency table is utilized to verify the dichotomous forecast (i.e., precipitation) over the Korean peninsula and the four combinations of the simulation and observation, called the joint distribution, is given in Table 6. The synthetic observational precipitation data is chosen as the reference data, and the data is linearly interpolated to 10-km and 40-km resolution to match with the model resolutions.

The accuracy, the critical success index, and the probability of detection all raised after applying two-way nesting method. Also, the false alarm rate drops slightly after applying two-way nesting method.

Table 5 The joint distribution of each experiment

	ICON w/o 2way	ICON 2way 40km	ICON 2way 10km
ACC	0.4969	0.5471	0.5343
CSI	0.4742	0.5283	0.5148
POD	0.4894	0.5471	0.5326
FAR	0.0613	0.0611	0.0609

IV. Conclusion

In this study, climatological simulation using ICON model with applying and without applying the two-way nesting method is performed, and the results are compared with other reanalysis and observational datasets to assess how does the fine grid resolution affect summer monsoon precipitation over the Korean peninsula. Also, showed the impact of feedback from the nested domain.

The finer spatial resolution exposes the high peaks of mountains more clearly. For example, the mountain Jiri which plays a major role in local precipitation derivated by geographical features.

In the zonal distribution, the ICON 2way 10-km depicts well the sharp peak of the precipitation at mountain Jiri, and due to the feedback, ICON 2way 40-km reproduced more amount of precipitation compared to ICON w/o 2way.

The impact of feedback is also showed up in the vertical structure. The downward motion derived from local orography became stronger in ICON 2way 40-km, and the weak downward motion over the East China sea shown in ICON w/o 2way disappears in the 2way experiments.

The NRMSE, Student's t-test, and Pearson correlation coefficient are applied to assess the difference between the two experiments, two-way nesting applied and not applied. There was an improvement after applying the two-way nesting method by

showing lower NRMSE and higher correlation coefficient at a significance level of 95%. Moreover, when applying the two-way nesting, the overall score of reproducing the dichotomous forecast was raised.

Thus, by applying two-way nesting method, the detail orography of nested domain improves the precipitation distribution, and through the feedback from the nested domain, this improvement also can be expected in the global domain.

V. References

Bae, H.J., and J.H. OH, 2017: Study of method for synthetic precipitation data for ungauged sites using quantitative precipitation mode. *Asia-Pacific Journal of Atmospheric Science,* **53**, 403-410, doi:10.1007/s13143-017-0038-z.

Dee, D. P., S. M. Uppala, A. J. Simmons, P. Berrisford, P. Poli, S. Kobayashi, U. Andrae, M. A. Balmaseda, G. Balsamo, P. Bauer, P. Bechtold, A. C. M. Beljaars, L. van de Berg, J. Bidlot, N. Bormann, C. Delsol, R. Dragani, M.Fuentes, A. J. Geer, L. Haimberger, S. B. Healy, H. Hersbach, E. V. Hólm, L. Isaksen, P. Kållberg, M. Köhler, M. Matricardi, A. P. McNally, B. M. Monge-Sanz, J.-J. Morcrette, B.-K. Park, C. Peubey, P. de Rosnay, C. Tavolato, J.-N Thépaut, and F. Vitart, 2011: The ERA-Interim reanalysis: configuration and performance of the data assimilation system. *Quarterly Journal of the Royal Meteorological Society*, **137**, 553–597. doi:10.1002/qj.828.

Harris, L. M., and S. Lin, 2014: Global-to-Regional Nested Grid Climate Simulations in the GFDL High Resolution Atmospheric Model. *Journal Of Climate*, **27(13)**, 4890-4910, doi:10.1175/JCLI-D-13-00596.1

Harris, L.M. and D.R. Durran, 2010: An Idealized Comparison of One-Way and Two-Way Grid Nesting. *Monthly Weather Review*, **138**, 2174–2187,

doi:10.1175/2010MWR3080.1.

Huffman, G.J., R.F. Adler, M.M. Morrissey, D.T. Bolvin, S. Curtis, R. Joyce, B. McGavock, and J. Susskind, 2001: Global precipitation at one-degree daily resolution from multi-satellite observations. *Journal of Hydrometeorology*, **2**, 36–50, doi:10.1175/1525-7541(2001)002<0036:GPAODD>2.0.CO;2.

Hurrell, J. W., J. J. Hack, D. Shea, J. M Caron, and J. Rosinski, 2008: A new sea surface temperature and sea ice boundary dataset for the Community Atmosphere Model. *Journal of Climate*, **21(19)**, 5145-5153, doi:10.1175/2008JCLI2292.1.

Kim, G.-Y., D.-H. Cha, G. Lee, C.-S. Jin, D.-K. Lee, M.-S. Suh, J.-B. Ahn, S.-K. Min, S.-Y. Hong, and H.-S. Kang, 2016: Impact of Horizontal Resolution on Precipitation Simulation over South Korea with Multi Regional Climate Models. *Journal of climate research*, 11(2), 169-181, doi:10.14383/cri.2016.11.2.169.

Kim, J. W., 2010: The impact of domain size and location in regional climate simulation, master's thesis, Retrieved from http://pknu.dcollection.net/jsp/common/DcLoOrgPer.jsp?sItemId=00000195 5764

Kitoh, A., and S. Kusunoki, 2008: East Asian summer monsoon simulation by a 20-km mesh AGCM. *Climate Dynamics*, **31(4)**, 389-401, doi:10.1007/s00382-007-0285-2.

Lee, Y. H., D. H. Cha, and D. K. Lee, 2008: Impact of Horizontal Resolution of Regional Climate Model on Precipitation Simulation over the Korean Peninsula. *Atmosphere*, **18(4)**, 378-395, doi:10.1175/MWR-D-14-00302.1.

Leung, L R, L. O. Mearns, F. Giorgi, and R. L. Wilby, 2003: Regional Climate Research. *Bulletin of the American Meteorological Society*, **84**, 89-95, doi:10.1175/bams-84-1-89.

Seong, M.G, S.G. Oh, and M.S. Suh, 2014: Simulation Skills of RegCM4 forced by ECHAM6 for Fine - scale Regional Climate over South Korea. *Journal of climate research*, **9(4)**, 283-302, doi:10.14383/cri.2014.9.4.283.

Wu, W., A. H. Lyncy, and A. Rivers, 2004: Estimating the Uncertainty in a Regional Climate Model Related to Initial and Lateral Boundary Conditions, *Journal of Climate*, **18**, 917-933, doi: 10.1175/JCLI-3293.1.

Zangl, G., D. Reinert, P. Ripodas, and M. Baldauf, 2015: The ICON (ICOsahedral Non-hydrostatic) modeling framework of DWD and MPI-M: Description of the non-hydrostatic dynamical core, *Quarterly Journal of the Royal Meteorological Society*, **141**, 563–579, doi:10.1002/qj.2378.